Nano Energy 70 (2020) 104459

Contents lists available at ScienceDirect

Nano Energy

journal homepage: http://www.elsevier.com/locate/nanoen

Full paper

A triboelectric and pyroelectric hybrid energy harvester for recovering energy from low-grade waste fluids

Dongyue Jiang [a,*], Yunpeng Su [a], Kun Wang [a], Yutao Wang [a], Minyi Xu [b,**], Ming Dong [a], Guijun Chen [a]

[a] Key Laboratory of Ocean Energy Utilization and Energy Conservation of Ministry of Education, Dalian University of Technology, 116024, China
[b] Marine Engineering College, Dalian Maritime University, Liaoning Province, 116026, China

ARTICLE INFO

Keywords:
Waste heat recovery
Low-grade waste heat
Triboelectric nanogenerator
Pyroelectricity
Droplet impact

ABSTRACT

Low-grade waste energy is widely available in industrial processes, and it typically appears in the form of thermal fluids. Types of technologies are developed for harvesting the thermal energy from these fluids. However, the thermal fluid not only possesses thermal energy, but also contains a large amount of kinetic energy. In this study, a hybrid device is proposed for harvesting both the thermal and kinetic energy of the thermal fluids. A free-standing type triboelectric nanogenerator (TENG) is employed for harvesting the kinetic energy, while a pyroelectric generator (PENG) is used for harvesting the thermal energy. Output performance of discrete water droplets with temperature of 5 °C, 25 °C, 45 °C and 65 °C are compared in both the TENG and PENG devices. The effects of the device inclination angle, and droplet released height are discussed. The analyses are conducted based on high-speed video recording of the droplet dynamics on the device as well as numerical simulation. The results indicate the droplet temperature, device inclination angle and droplet released height affect the droplet dynamics significantly. Further, the variation of droplet dynamics greatly affects the output performance of both the TENG and PENG. The peak output power of the TENG decreases with the increase of droplet temperature, while the output power of the PENG increases with the temperature variation. A hybrid energy harvester was fabricated and a peak power density of 2.6 μW/cm^2 was achieved. A maximum energy increment of 238% was obtained by the hybrid harvester, as compared to the pure PENG device. The harvested energy was able to light up 28 commercial LED light bulbs.

1. Introduction

Low-grade waste heat resources (temperature below 130 °C) are widely available in geothermal and industrial sectors including: power plants, chemical plants, oil refineries, steel/glass/metal productions and so on [1–3]. Low-grade waste heat is typically discarded in the industrial sectors due to the limitations (less efficient, low cost-effectiveness) in the recovery technology. Around 20–50% of the energy input in the industrial sectors is lost as low-grade waste heat in the forms of water, vapor and gas [4]. Such a large amount of low-grade thermal energy discharge has led to serious energy waste as well as environmentally unfriendly thermal pollution [5].

There are several ways for low-grade waste heat recovery such as Organic Rankine Cycle (ORC) [6–8], heat pumps [9–11], solid-state power converters [12–15] (thermoelectrics, pyroelectrics, near-field thermophotonic systems etc.) and electrochemical methods [16–18] (thermocells: thermoelectrochemical cells, thermos-osmotic systems, thermally regenerative batteries *etc.*). ORC technology was developed in 1950s, aiming at utilizing the organic working fluids with a liquid-vapor phase change property for replacing water/steam to complete the Rankine cycle [19]. The selection of the working fluid is of great importance because the reduced phase change temperature of the working fluid may lead to heat transfer deterioration [20]. Besides, the organic working fluid could be toxic and harmful to the environment [21]. Similarly, heat pump systems also face the challenges of refrigerant selection, sealing problem and ozone layer protection [22]. The thermocells operate with the temperature dependence of electrochemical redox potentials to provide power with the low-grade waste heat [23]. However, the thermocells face the problems of high material cost and complicated electrodes fabrication, as well as the low

* Corresponding author.
** Corresponding author.
E-mail addresses: jiangdy@dlut.edu.cn (D. Jiang), xuminyi@dlmu.edu.cn (M. Xu).

https://doi.org/10.1016/j.nanoen.2020.104459
Received 18 October 2019; Received in revised form 14 December 2019; Accepted 28 December 2019
Available online 7 January 2020
2211-2855/© 2020 Elsevier Ltd. All rights reserved.

Carnot-relative efficiency [24]. Among these technologies, solid-state pyroelectric generators utilize the temporal temperature variation (dT/dt) on the pyroelectric material for power conversion show great potential [25]. Under correct working conditions, they have the potential to operate with a higher thermodynamic efficiency, as compared to thermoelectric generators. The feature of converting heat sources with temperature oscillation into power makes pyroelectric a good candidate for harvesting energy from a period heat source. Several demonstrations have been proposed for power conversion from heat sources including solar/wind flow, body heat, waste heat *etc.* [26–28].

In practical applications, the low-grade thermal energy generally appears in the form of condensed water, containing not only thermal energy but also a large amount of kinetic energy. For example, the condensed water drops in the rain zone in the hyperboloid cooling tower (an important component in power plant) and the hot stream in the pipe network *etc.*, both contain thermal as well as kinetic energy. Hence, it is essential to harvest both the thermal and kinetic energy of the low-grade waste fluids to improve the output power. Triboelectric nanogenerators (TENG) developed by Prof. Zhong Lin Wang's group have been demonstrated with good capabilities in mechanical energy harvesting [29–39]. Based on TENG device, various applications have been developed and the output power has been boosted significantly [40]. In recent years, several solid-liquid based triboelectric nanogenerators are proposed for harvesting the kinetic energy from sliding drops, flowing streams, ocean waves, and so on [41–51]. The solid-liquid TENG devices open up opportunities in harvesting the kinetic energy from hot fluids. The achievements made by peer researchers in solid-liquid TENG and liquid PENG are listed in Table 1. Besides, several hybrid cells are proposed for harvesting the thermal and kinetic energy from solid-solid interaction [52–64]. However, the demonstration of hybrid devices recovering thermal and kinetic energy from hot fluids has been omitted.

In this study, a hybrid triboelectric and pyroelectric energy harvester (TPENG) for recovering the energy from low-grade waste fluids is proposed. The pyroelectric energy harvester could be employed for recovering the low-grade thermal energy, the triboelectric nanogenerator targets on harvesting the kinetic energy of hot fluids. A 2.6 μW/cm^2 output power density was reached when 65 °C droplets were dripped onto the device, and the output power of the device is able to light up 28 commercial LEDs.

2. Results and discussion

2.1. Concept and working principle of the TPENG

This study investigates the energy harvesting from the hot droplets in industrial processes. In order to clarify the concept, a hyperboloid cooling tower is drawn in Fig. 1a for illustration. The hot droplets are originated from the spray nozzles of the hyperboloid cooling towers. The TPENG is formed by a free-standing mode TENG device (the 1st hydrophobic layer (Fluere-1710, Sino-Fluorine) and the 2nd silver electrode layer) and the pyroelectric device (the 4th silver electrode layer, the 5th polarized-PVDF layer and the 6th silver electrode layer). The TENG device and the pyroelectric device are separated by the 3rd insulation layer (Kapton tape). The detailed working principle is shown in Fig. 1b. For the TENG device, the negative charges accumulate on the hydrophobic layer after interaction with water droplets. The charges on the hydrophobic layer are in electrical equilibrium with the silver electrode underneath (stage <I>). When a subsequent hot droplet touches the device, the negative charges on the hydrophobic layer attracts the cations from the droplet and an electrical double layer (EDL) is formed. The excessive positive charges on the top silver electrode move to the bottom and a current flow through external circuit is formed (stage <II>). When the droplet slides down to the bottom electrode (stage <III>), a same process is repeated and a reverse current could be obtained. For the pyroelectric generator, the polarized PVDF possesses dipoles aligning perpendicularly to the thin film as shown in stage <I>. The dipoles are originated from the fluorine atoms (negative) facing up and hydrogen atoms (positive) [71]. The aligned dipoles are in electrical equilibrium with silver electrodes. When the hot droplet contacts the surface of the TPENG, heat is transferred to the pyroelectric layer and the dipoles of molecules oscillate within a larger degree of oscillation angles, which is due to the thermally induced random wobbling of the dipoles around its axes. As a result, the surface polarization intensity of the PVDF thin film reduces. Similarly, when heat is dissipated from the pyroelectric layer, these dipoles tend to oscillate within a small angle as the thermally induced random motion is suppressed [53]. As shown in stage <II> of pyroelectric generator, the reduced polarization of the PVDF film yields a current flow from the 4th silver electrode layer to the 6th electrode layer. The current flow stops when the thermal energy is dissipated to the environment.

2.2. Output performance of the TENG

Fig. 2 presents the output performance of the TENG device when droplets with varied temperature drip onto the inclined energy harvester (30 mm × 80 mm). In order to eliminate the influence caused by the pyroelectric and piezoelectric effect, a pure free-standing TENG device is fabricated with silver electrodes and hydrophobic layer (Sino-Fluorine Fluere-1710, 600 nm). The preliminary experimental test is conducted at room temperature (25 °C). De-ionized water droplets are ejected by a syringe pump at an interval of 18 s. The droplet size is kept as 30 μL throughout the experiment. Fig. 2a–c shows the open-circuit voltage, short-circuit current and transferred charges when sequential droplets drip onto the TENG device. In this test, the inclination angle of the TENG device is $\alpha = 45°$. The droplet is released right above the TENG device ($H = 0$ cm). It is seen that an 18 V peak-to-peak open-circuit voltage and 3.2 μA short-circuit current are obtained by a single droplet. The transferred charges induced by the first droplet is the largest, and stabilizes from the fourth droplet. As shown in Fig. 2a, after obtaining a negative peak signal by the sliding droplet, a slow recovery of the voltage signal is observed. This is because the tribo-charges accumulated on the TENG surface require a duration to be dissipated.

After obtaining the reference data of the TENG device, the effects of the droplet temperature, droplet released height and the inclination angle of the TENG device are investigated. In this test, the inclination angle (α) of the device is controlled by a rotating stage at the range of 30–60°, with an interval of 15°. The droplet temperature (T_{drop}) is controlled by a Peltier heating/cooling unit at the range of 5–65 °C, with

Table 1
List of achievements in solid-liquid TENG and liquid PENG devices.

Number	Source	Working mode	Power density (μW/cm^2)	Temperature difference (K)	Application	Reference
1	Droplet	TENG	9.1	N.A.	Energy harvesting	[42]
2	Droplet	TENG	50	N.A.	Energy harvesting	[65]
3	Droplet	TENG	0.3	N.A.	Energy harvesting	[66]
4	Droplet	TENG	0.27	N.A.	Hybrid solar cell	[67]
5	Droplet	TENG	8	N.A.	Smart umbrella	[68]
6	Stream	PENG	14	80 K	Energy harvesting	[15]
7	Water vapor	PENG	4.12	30 K	Energy harvesting	[69]
8	Liquid interface	PENG with bias electric field	110 (mW/cm^3)	80 K	Energy harvesting	[70]

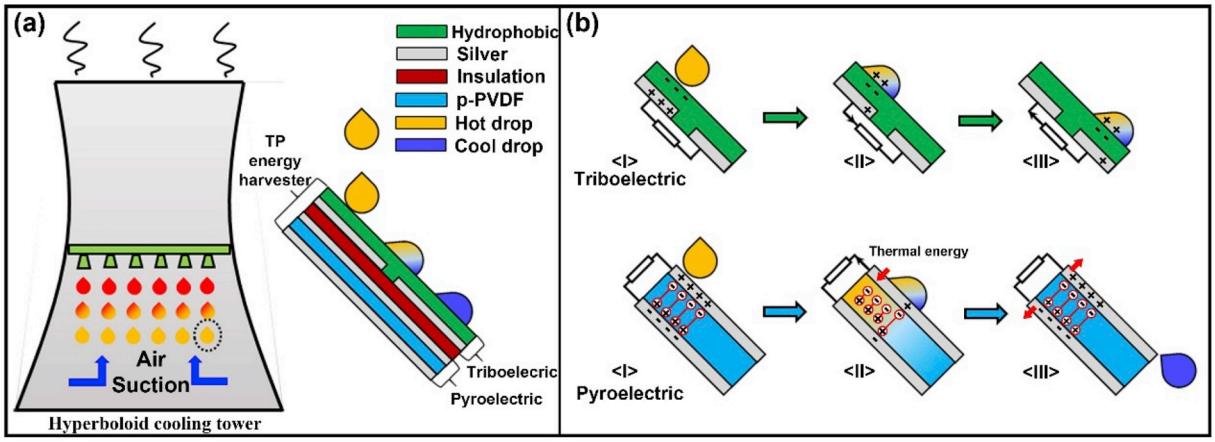

Fig. 1. (a) Schematic diagram of the TPENG and (b) Detailed working principle of the triboelectric, and pyroelectric generators during interaction with a hot water droplet.

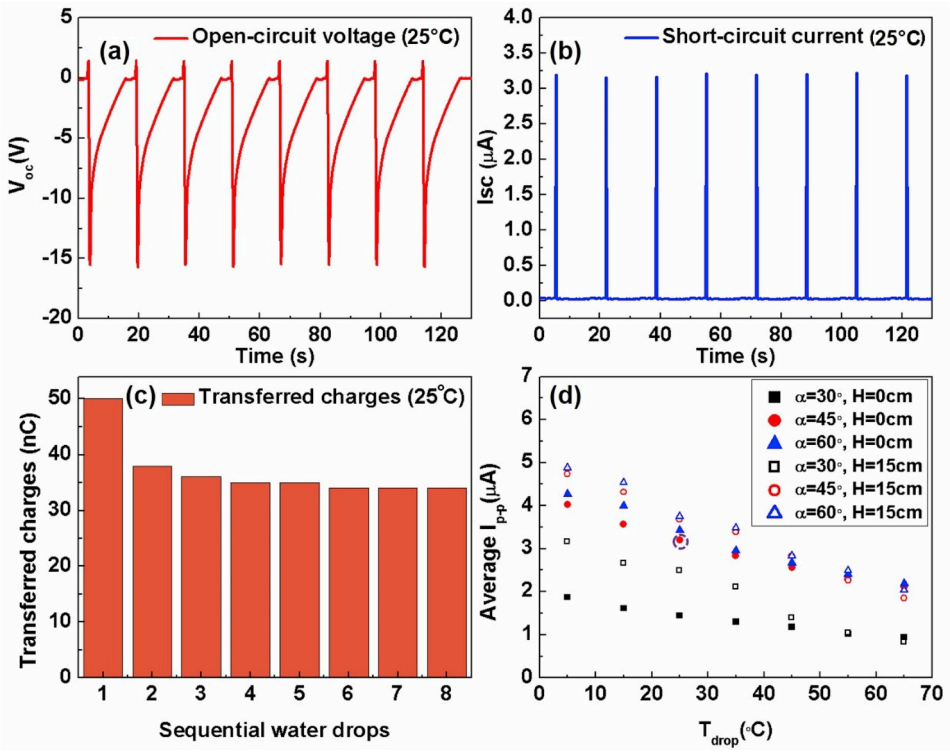

Fig. 2. Output performance of the TENG device: (a–c) open-circuit voltage, short-circuit current and transferred charges when a 30 μL, 25 °C droplet slides down a 45° inclined TENG device (H = 0 cm); (d) effects of device inclination angle (α), droplet temperature (T_{drop}) and released height (H) on the output current of TENG device.

an interval of 20 °C. A FLIR thermal imager is employed to monitor the temperature of the droplet during the experiment. The released height (H) is varied by an adjustment stage between 0 and 15 cm. As shown in Fig. 2d, no matter how α and H vary, the $I_{p\text{-}p}$ reduces with the increase of droplet temperature. This decreasing trend was obtained in a previous contact-separation mode TENG device [45] and the reason was explained by the reduced dielectric constant and polarity of water at elevated temperatures [72]. These reasons well explained the reduction of output performance in a contact-separation mode TENG. However, in a freestanding mode TENG device, the temperature induced density, surface tension and viscosity variation of water could not be omitted. These factors significantly affect the droplet dynamics on the TENG device. In order to examine these influences, a high speed imaging (Photron Mini UX50) test of the droplet dynamic motion on the TENG device was carried out.

Fig. 3 presents the sequential snapshots of droplet shapes during transportation on the free-standing TENG device. It is seen that no matter how H and α vary, the hot droplets (65 °C) spend a longer duration than the cool droplets (5 °C). This is because the surface tension of a hot droplet (65 mN/m) is much lower than the cool droplet (75 mN/m). The lower surface tension of the hot droplet yields a smaller contact angle (inset of Fig. 3c and d) and larger contact area. The increased contact area induces larger resistive force during the droplet transportation. It is known that the output performance of the TENG device is inversely proportional to the duration of charge transfer (dq/dt), the cool droplets with shorter transportation duration would induce a

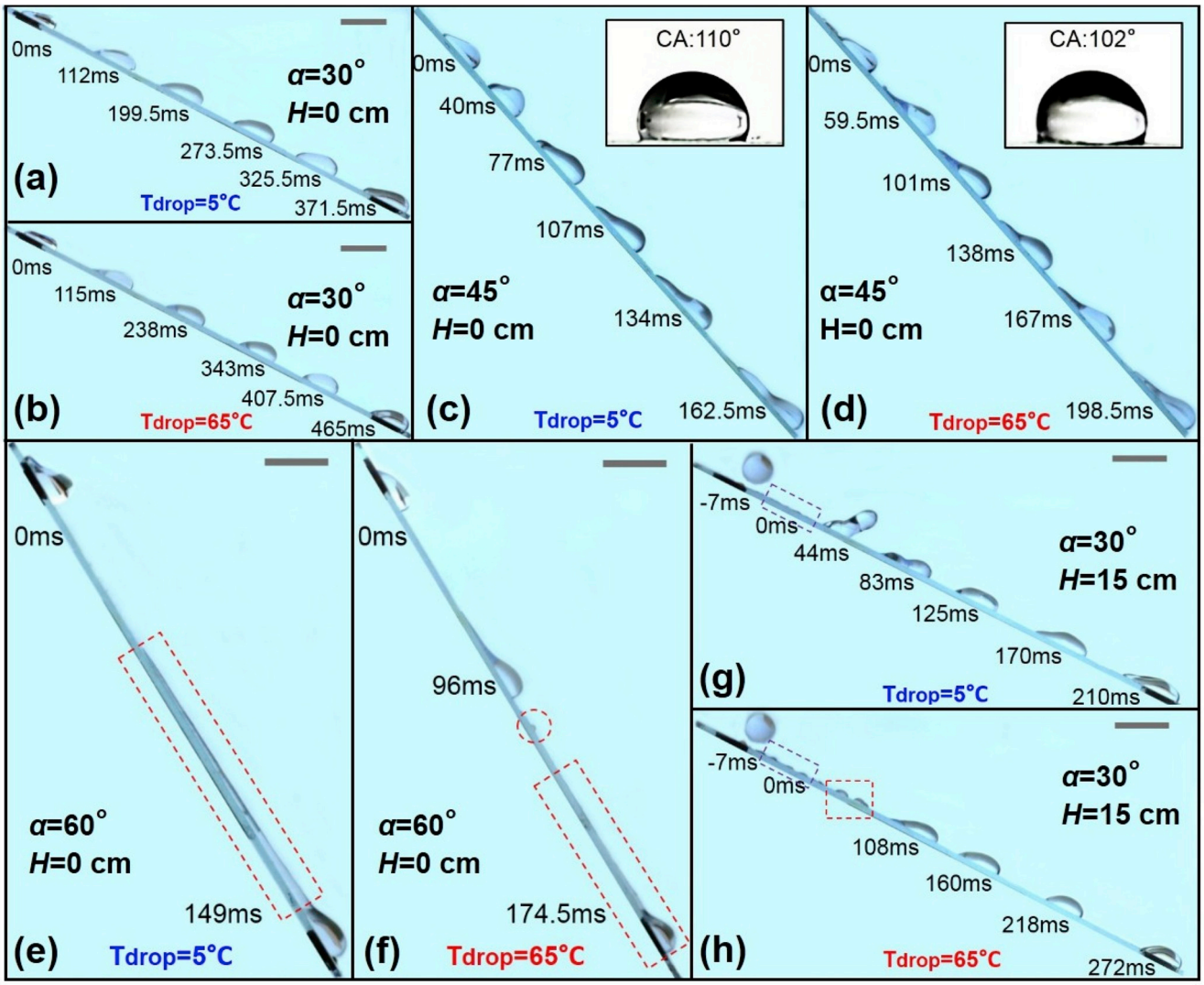

Fig. 3. Dynamics of droplets sliding hydrophobic surfaces: (a) 5 °C, α = 30°, H = 0 cm, (b) 65 °C. α = 30°, H = 0 cm, (c) 5 °C, α = 45°, H = 0 cm, (d) 65 °C. α = 45°, H = 0 cm, (e) 5 °C, α = 60°, H = 0 cm, (f) 65 °C. α = 60°, H = 0 cm, (g) 5 °C, α = 30°, H = 15 cm, (h) 65 °C, α = 30°, H = 15 cm.

higher output. It is noteworthy that the increase in the contact area is favorable in obtaining a higher output in the TENG device. However, the effect of velocity is the dominant as compared to the effect of contact area increase [73]. Another major effect shown in Fig. 2d is the inclination angle α of TENG device. It is seen that with the increase of α from 30° to 45°, the output performance increases significantly, while α increases from 45° to 60°, the peak current increment is not obvious. This could also be explained by the snapshots of the droplet dynamic motions. As shown in Fig. 3a–f, the cool and hot droplets are transporting on 30°, 45° and 60° inclined TENG devices ($H = 0$ cm), respectively. The duration of the droplet transportation process follows a trend of: $t_{30°} > t_{45°} > t_{60°}$. This is because the slip component of the gravitational force is larger on a highly inclined surface. This explains the significant current increase when α from 30° to 45°. Another explanation on the effect of TENG device inclination angle is the contact area. For a cool droplet at 5 °C, it is seen from Fig. 3a, c, and e that the droplet spread area on the TENG device increases with inclination angle. A very long tail of the droplet could be observed in Fig. 3e on a 60° inclined surface. This is because during the droplet impact process, the kinetic energy is dissipated by the droplet surface energy during droplet spread out as well as the viscous energy within the droplet. When the slip component of the gravitational force increases, the force tends to stretch the droplet and yields a larger contact area. This increased contact area induces an overlap of the droplet with both the upper and lower electrodes, yielding a cancelling out of the output current. This explains the less significant increment of the output current when the device inclination angle exceeds 45°. For a droplet with the temperature greater than 45 °C, the output current obtained on a 60° inclined surface is comparable with that obtained on a 45° inclined surface. This is because the surface tension of water reduces when the temperature increases. When a hot droplet drips on a highly inclined surface, the gravitational force tends to pull the droplet with a larger contact area. However, due to the reduced surface tension, the hot droplet is easily broken and yields tiny droplets on the TENG surface as shown in Fig. 3f (red circle). The tiny droplet stays on the TENG device without an effective friction and weakens the output current of the TENG device. Considering the real applications where multiple water droplets would drip onto the TENG device simultaneously, uneven sized upper and bottom electrodes or single-electrode mode TENG devices can be proposed to avoid the cancelling out effect. In terms of the droplet released height H, as shown in Fig. 2d, the output performance of the droplet released at $H = 15$ cm are larger than those obtained at $H = 0$ cm (empty dots are higher than full dots). This is due to the larger potential energy when the released height is increased. Such a high potential energy is beneficial for the droplet obtaining a high speed and short transportation on the TENG device. Exceptions reveal when the droplet temperature increases. This

could also be attributed to the reduced surface tension of the hot droplets. As shown in Fig. 3h, when a hot droplet impacts on a 30° inclined TENG device from a height of 15 cm, the droplet breaks during the retraction process and leaves several satellite droplets which made adverse effect to the output current.

The droplet induced contact electrification is a combination of a droplet impact process and a triboelectrification process. In the droplet impact process, the droplet falls from a certain height to the TENG device surface, then spreads out and followed by a refraction and sliding motion. The maximum contact area of the droplet could be estimated by an energy balance equation when $We < 1000$ [74]:

$$A_{\max} = \frac{\pi}{4} D_0^2 \times \frac{We + 12}{3(1 - \cos\theta_a) + 4We/\sqrt{\mathrm{Re}}} \quad (1)$$

In which $A_{\max}$ is the maximum spread area of the droplet when drips on a inclined surface. D_0 is the droplet diameter, Dimensionless Weber number $We = \rho v^2 D_0/\sigma$ characterizes the ratio of inertial force and surface tension, ρ and v represent the density and velocity of the droplet. θ_a is the advancing angle of the droplet when drips on an inclined surface. Dimensionless Reynolds number $Re = \rho v D_0/\mu$ describes the ratio of inertial force and viscous force, μ is the dynamic viscosity. Based on the maximum spread area model, the droplet induced triboelectric current could be expressed as:

$$I_{TENG} = A_{\max} \frac{d\sigma_I}{dt} \quad (2)$$

From Equation (2) we can find the output current increases with We, which indicates that a larger initial speed of the droplet not only reduces the transportation duration, but also contributes a larger contact area. Besides, on a highly inclined surface, the advancing contact angle is small, which yields a larger contact area. The trend in Equations (1) and (2) well matches the experimental observations. It is noteworthy that Equations (1) and (2) only accounts for the cases that there is no droplet breakings during the impact motion. Besides, the output performance of the TENG device is heavily dependent on properties of water droplets. This section comprehensively investigated the effects of droplet temperature, device inclination angle and droplet released height. There are also other parameters affecting the surface tension, viscosity, density as well as tribo-charges formation between the liquid and solid interface. Previous studies [75–77] have investigated the surface tension and viscosity of water varying with pH value, salt type and concentration. Besides, the output performance of TENG devices are examined in terms of pH value, ion type and concentration in Refs. [78–81]. The results revealed that an increase in ion concentration would decrease, while an increase in pH value would increase the output performance of TENG devices.

2.3. Output performance of the pyroelectric energy harvester (PENG)

The previous section discusses the output performance of the TENG device. Here the output performance of the PENG is examined. A PENG device (detail could be seen from the inset of Fig. 4a, 30 mm × 80 mm) is assembled by a 110 μm thick p-PVDF thin film, top and bottom silver electrodes (6 μm thick), as well as a hydrophobic layer (200 nm) above the top silver electrode. It is noteworthy that the hydrophobic layer and the top silver electrode forms a single-electrode mode TENG device. In order to eliminate the effect of the triboelectric output, a Cytop (FluoroPel PFC1101V) hydrophobic layer with a very low triboelectric output (Fig. S1) is employed. The thin hydrophobic layer possesses a low surface energy (droplet static contact angle of 110°) which ensures a fast droplet sliding motion on the PENG device as well as low thermal resistance to the heat transfer. The output performance of the PENG is examined in terms of droplet temperature (T_{drop}), device inclination angle (α), and droplet released height (H). The droplet size is maintained as 30 μL. The droplet temperature is continuously monitored by a thermal imager as shown in the inset of Fig. 4. The p-PVDF material

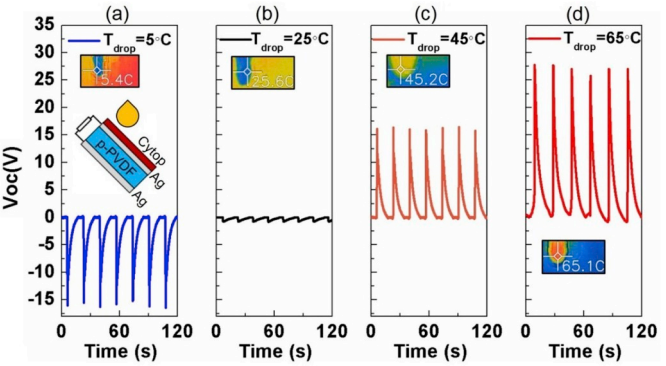

Fig. 4. Open-circuit voltage of PENG obtained by droplets with different temperatures: (a) 5 °C, (b) 25 °C, (c) 45 °C and (d) 65 °C. Droplet size: 30 μL, PENG device inclination angle $\alpha = 45°$, droplet released height $H = 0$ cm.

possesses both the pyroelectric and piezoelectric output properties. The output from the PENG device is the combination of the two effects. In order to distinguish the output of the pyroelectric and piezoelectric effect, a room temperature droplet with a 0 °C temperature difference is adopted first. As shown in Fig. 4b, when a room temperature (25 °C) droplet is released at the height of 0 cm, an open-circuit voltage of ~-1 V is obtained. This voltage is mainly originated from the piezoelectric effect when the droplet drips on the PENG surface, as there is no temperature difference between the droplet and the PENG device. Once a temperature difference is applied, the open-circuit voltage changes significantly as shown in Fig. 4a, c and 4d: when a droplet with temperature lower than the PENG device, negative peaks could be obtained, while a droplet with higher temperature impacts on the PENG device, positive peaks could be attained. When there is a 40 °C temperature difference between the droplet (65 °C) and the PENG device (25 °C), a 27 V average open-circuit voltage could be measured with a single 30 μL droplet. As compared to the output performance of the pyroelectric generator, the piezoelectric output is negligibly small. The short-circuit current of the PENG device are plotted in Fig. S2 and the current signal follows the trend of the open-circuit voltage. The output current of the PENG could be expressed as:

$$I_{PENG} = pAdT/dt \quad (3)$$

In which p is the pyroelectric coefficient, A is the contact area between hot droplet and PENG surface, and dT/dt is the rate of temperature change of the PENG device. The measured data is in good agreement with the output current model in Equation (3). It is noteworthy that the pyroelectric effect is triggered by the temporal temperature variation within the PENG device. When a continuous high temperature stream drips onto the PENG device, the output signal would vanish (as shown in Fig. S3 in the supporting information) as the entire device is heated (a thermal equilibrium condition) and the temperature variation within the PENG device does not exist anymore. In real applications when droplets are dripping onto the device tightly, a heat sink could be employed to quickly dissipate the heat transferred by the previous droplet, so that a temperature variation could be established when the next hot droplet arrives.

For a detailed investigation on the heat transfer performance of the PENG device, a numerical simulation is conducted by Comsol Multiphysics. Fig. 5 shows the transportation process of a 65 °C droplet on a 45° inclined surface. As compared to the high speed camera captured images presented in Fig. 3d, the droplet dynamic motion generally follows the experimental data in terms of droplet shape variation as well as total transportation duration. The temperature profiles of the top layer of the PENG device at t = 0, 100 and 200 ms are plotted in the inset of Fig. 5. At the moment of t = 0 ms, the droplet impacts on the left part of the PENG device and the temperature increases at the region where the droplet impacts. This temperature increase on the top layer of the PENG

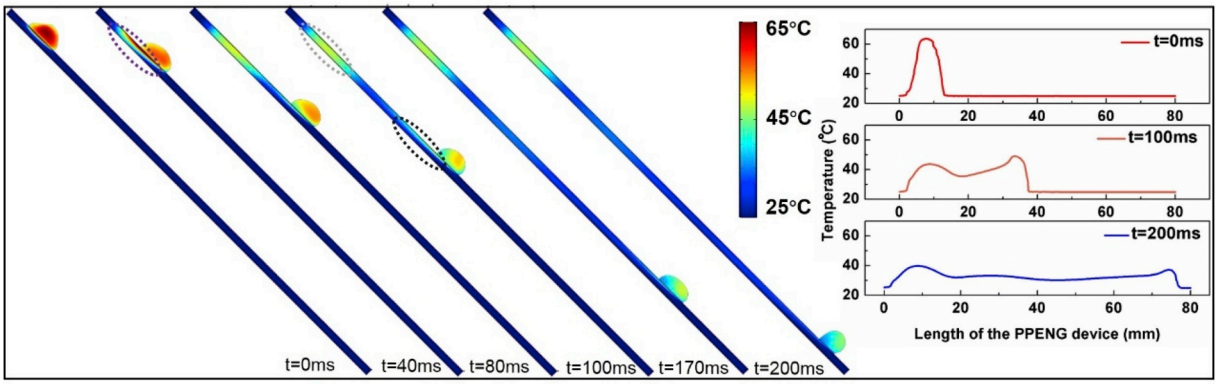

Fig. 5. Temperature distribution of the droplet and PENG device at different moments.

device would induce a temperature difference (purple circle in Fig. 5) as the bottom surface of the PENG is in contact with the glass substrate at 25 °C. The temperature variation contributes to the pyroelectric output. At the middle and right parts of the device (Length 20–80 mm), the top surface temperature remains the same as the room temperature and does not contribute to the power output. At the moment of t = 100 ms, the droplet transports to the middle part of the device (Length 30–40 mm), the local surface of the PENG device is heated by the droplet. This heating effect also induces a temperature variation (black circle in Fig. 5) and contributes to the power output. As the temperature of the droplet reduces during the transportation process (thermal conduction, convection and radiation heat transfer to both the device and the environment), the temperature variation at the middle part of the device is not as large as the left part. At this moment, one can find the left part of the device still maintains a high top surface temperature. However, this high temperature does not contribute to the power output anymore, as the heat is conducted from the top to the bottom at the left part of the device and the temperature variation vanishes (gray circle in Fig. 5). One can conclude from the simulation results that the initial point where the droplet impacts contributes more to the power output. Besides, the droplet transportation is beneficial for power output as it creates more area with temperature variations.

Fig. 6a presents the effects of α, H and T_{drop} on the average peak-to-peak open-circuit voltage of the PENG. The full dot shows the situation when the droplet is released from a height of $H = 0$ cm, while empty dot represents a droplet released height of $H = 15$ cm. The PENG device inclination angle α are represented by different colors: $\alpha = 30°$, black; $\alpha = 45°$, red; $\alpha = 60°$, blue. Similar to the trend presented in Fig. 4, when a larger temperature difference is applied ($T_{drop} = 5$ °C, 65 °C), a larger absolute open-circuit voltage could be obtained. In terms of the PENG inclination angle α, larger absolute open-circuit voltage values are attained at smaller α cases. This could be attributed to the droplet dynamics motion on the PENG. As shown in Fig. 3a–f, the droplet transportation speed on a low inclination angle surface is lower than that on a high inclination angle surface. The reduced speed ensures a longer duration and a more intensive heat transfer between droplet and the PENG surface. This could also be proved by the time lapsed thermal snapshots of the surface temperature distribution shown in the top row of Fig. 6b. It is seen that the surface temperature of PENG gradually reduces after a 65 °C droplet impact. On a $\alpha = 30°$ surface (bottom row of 6b), the duration for the surface fully returns to room temperature is 18 s, while only 12 s is required on a $\alpha = 60°$ surface. Another trend in Fig. 6a is that when the droplet is released from a height of $H = 15$ cm, the output voltage is larger than the value obtained by $H = 0$ cm. It is seen from Fig. 3g and h that the droplet transportation speed is increased when $H = 15$ cm. This may induce a heat transfer deterioration between the droplet and the PENG surface. However, when a droplet is released from the height of $H = 15$ cm, the droplet would spread to a larger area as shown in the purple square (0 ms) in Fig. 3g and h. This large spread area of the droplet is due to the conversion of larger inertial force at $H = 15$ cm into surface tension and viscous dissipation. Such a large spread area would induce a stronger heat transfer and the initial temperature variation contributes more to the output as presented in Fig. 6a. With these two effects, the total heat transfer is enhanced by a larger released

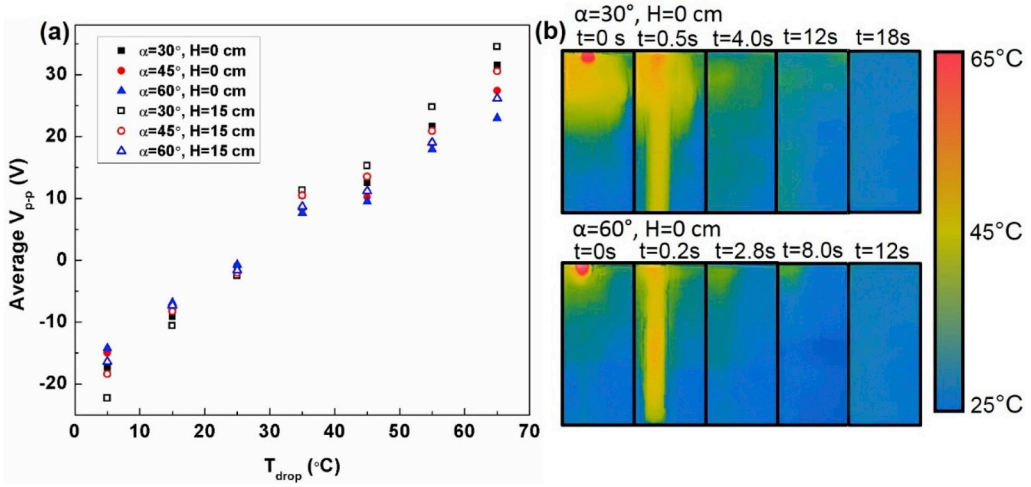

Fig. 6. (a) Output performance of the PENG device affected by the device inclination angle (α), droplet temperature (T_{drop}) and released height (H) and (b) sequential thermal imager captured figures showing the temperature distribution on the PENG device at varied inclination angles: top row, $\alpha = 30°$, bottom row, $\alpha = 60°$.

height of $H = 15$ cm, as compared to a height of $H = 0$ cm.

2.4. Output performance of the TPENG hybrid cell

From the results presented in the previous sections, it is found the output performance of TENG device increases with the droplet transportation speed, while that of the PENG reduces with the droplet speed as an efficient heat transfer is desired. In order to maximize the output performance of the TPENG, released height of $H = 15$ cm is adopted as it ensures a fast droplet motion and good heat transfer as a large spread area could be obtained when the droplet is released from a larger H value positon. A detailed comparison of TENG and PENG as a function of H could be found from Fig. S5. In terms of inclination angle, $\alpha = 45°$ is adopted for balancing the droplet transportation speed and heat transfer performance. The output power and energy of the TPENG are measured based on single droplet impact motion. Load resistances ranging from 0.1 to 2000 MΩ are swept for obtaining the maximum output power. In terms of the TENG device (Fig. 7a), the highest output power of 3.76 μW is obtained when the droplet temperature is 5 °C and load resistance of 50 MΩ, which is consistent with the results shown in Fig. 2d. In terms of the PENG, the trend of the peak output power generally follows that of the temperature difference and the peak output power is lower than the TENG even a 65 °C droplet is applied (Fig. 7b). The output power was calculated by the production of peak current square and the load resistance, the results indicate that the TENG generates larger peak power except for the case when the droplet temperature is 65 °C. In terms of the output energy of TENG and PENG devices, the trend might be different as the duration of the current signal also takes effect. The TENG and PENG output currents obtained by a 5 °C droplet and 20 MΩ load resistance are plotted in Fig. 7c. It is seen a high but narrow current signal is obtained by the TENG, while a low but wide current signal is produced by the PENG. These two current signals are in good agreement with the output current obtained by the TPENG hybrid cell (parallel connecting the output terminals of both TENG and PENG) at the same condition (Fig. 7d). The output energy is attained by evaluating the integral of output power over time. As shown in Fig. 7e–h, the output energy of the hybrid cell is composed of the output energy induced by the TENG and PENG devices. When the droplet temperature is lower than 45 °C, the TENG device dominates the energy output, while the PENG dominates the energy output when the droplet temperature is 45 °C and 65 °C. This is attributed to the reduced performance of the TENG device at high temperature conditions as well as the larger temperature difference applied to the PENG. As compared to the pure PENG output, the hybrid harvester enhanced the output energy of 238%, 33.9% and 12.1% when the droplet temperatures are 5 °C, 45 °C, and 65 °C, respectively. In the TPENG device, the TENG and insulation layer would induce a heat transfer deterioration due to the thermal resistances. A temperature test was conducted on the TPENG device and the result is presented in Fig. S4. Initially, due to the existence of the thermal resistances caused by TENG and Kapton layer, a large temperature difference is observed between droplet and PENG device. With the increment of time of ~10 s, the heat transfer tends to be a steady state and a temperature difference of <1 K is observed between the droplet and the PENG device. Considering the real applications where the hot droplets are dripped onto the TPENG with short intervals, such a small temperature difference incurred by the thermal resistances could be ignored.

A TPENG with a size of 30 mm × 200 mm is fabricated for the demonstration of lighting up commercial LED light bulbs. A maximum power density of 2.6 μW/cm^2 was obtained when a 40 °C temperature difference is applied. The output terminals of the PENG was connected with a full wave rectifier and used to light up 21 LED light bulbs (forming a pattern "DU"), while the TENG device was used to light up 7 LED light bulbs (forming a pattern of "T"). Similar to the trend presented in Fig. 7c and d, the formed "T" pattern shines with a short duration, while the pattern "DU" maintains longer (as shown in the Supporting movie).

Supplementary video related to this article can be found at https

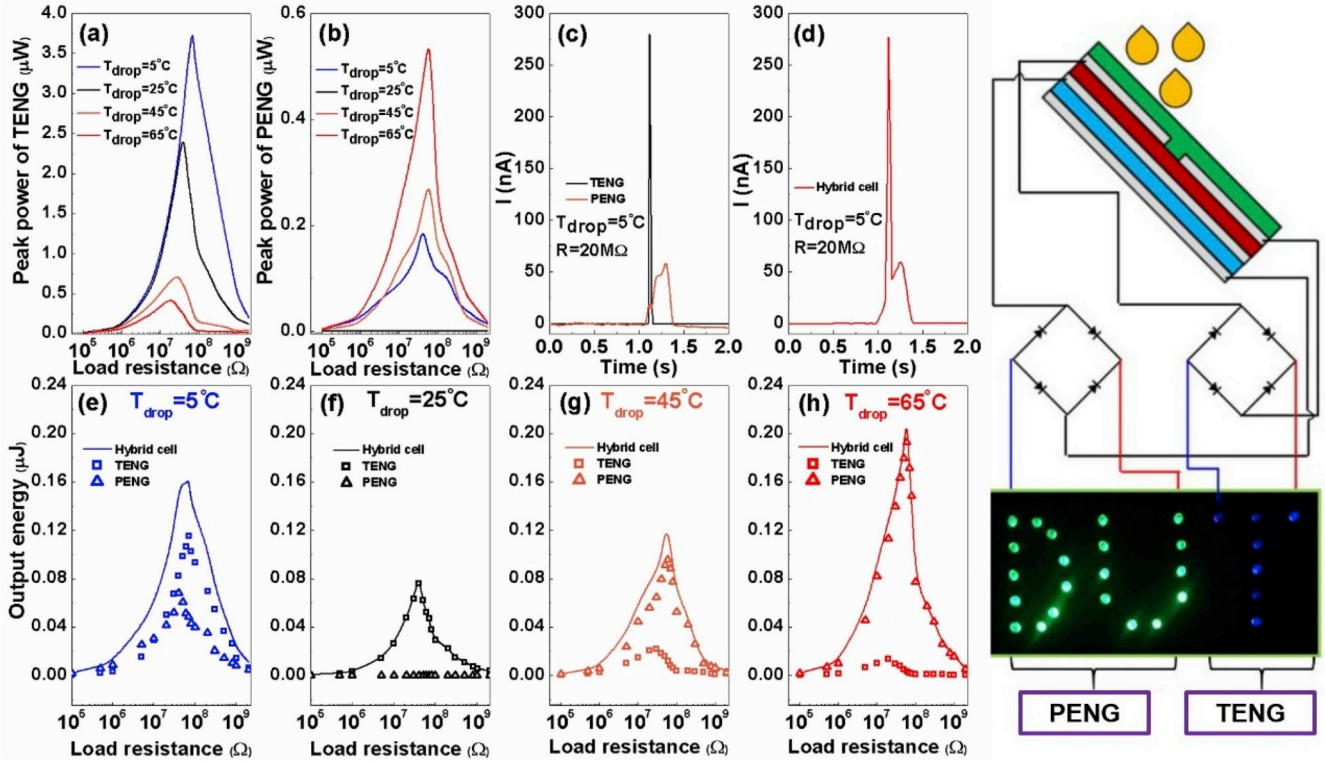

Fig. 7. Peak output power of TENG (a) and PENG (b), current of TENG, PENG and hybrid cell at $T_{drop} = 5$ °C and load resistance of 20 MΩ (c–d), output energy of the TENG, PENG and TPENG when the droplet temperature is 5 °C (e), 25 °C (f), 45 °C (g) and 65 °C (h).

://doi.org/10.1016/j.nanoen.2020.104459.

3. Conclusion

This study proposed a TPENG for recovering both the thermal and kinetic energy of low-grade thermal droplet. The kinetic energy of the droplet is harvested by the TENG. The output performance of the TENG is found to increase with the decrease of droplet temperature, increase of droplet released height and device inclination angle. The underlying mechanism is investigated by a high speed video and the droplet dynamics is found to play an important role in the TENG output performance. In terms of the PENG, the output performance is found to increase with the increase of temperature difference between the droplet and environment, droplet released height and decrease of device inclination angle. The droplet transportation speed and heat transfer performance both affect the output performance of the PENG. The output power and energy of the TPENG are measured with varied droplet temperature and load resistances. A peak output power of 3.76 μW and 0.52 μW was obtained by the TENG (5 °C droplet) and PENG (65 °C droplet). However, the duration of the peak power induced by the TENG is much shorter than that of PENG. As a result, the output energy shows a different trend: when the droplet temperature is low (5 °C and 25 °C), the output performance is dominated by TENG, while the PENG dominates the output energy when the droplet temperature is increased to 45 °C and 65 °C. A maximum energy increment of 238% was obtained by the hybrid harvester, as compared to the pure PENG device. By parallel connecting the TENG and PENG, the TPENG is employed for lighting up 28 LED lightbulbs and a peak power density of 2.6 $\mu W/cm^2$ is measured.

4. Methods

Device fabrication: The pure TENG device is fabricated by dip coating Fluere-1710 (600 nm) onto a piece of glass (30 mm × 80 mm) with two silver electrodes (each electrode 30 mm × 39 mm × 6 μm, a gap of 2 mm is between the two electrodes). The pure PENG is fabricated by spin coating Cytop (FluoroPel PFC1101V, 200 nm) onto a commercial p-PVDF film (TE Connectivity, 110 μm). The TPENG is fabricated by sticking a Kapton tape on one side of the commercial p-PVDF film, coating silver electrodes on the Kapton tape, and dip coating Fluere-1710 on top of the room temperature cured silver electrodes. The droplet is generated by a syringe pump connected needle and the temperature of the droplet is maintained by a Peltier cooling/heating unit.

Characterization: The thickness of the Fluere-1710 hydrophobic layer, silver electrodes, and Cytop hydrophobic layer are conducted by a step profiler (KLATencor Alpha-step stylus profiler).

Measurement: The motion of the water droplet is captured by a high speed camera (Photron Mini UX50) and the frame rate is set as 2000 fps at a full resolution. The output current, voltage and charge signals are measured by a Keithley 6514 electrometer. The contact angle measurement of the actuation droplet was conducted by ImageJ software. A FLIR thermal imager is employed for monitoring the droplet temperature throughout the experiment to ensure consistency.

Numerical simulation: Laminar flow, heat transfer in solid and fluids, and level set multiphysics model is employed to analyze the droplet dynamic motion as well as heat transfer.

Declaration of competing interest

The authors declare that they have no known competing financial interests or personal relationships that could have appeared to influence the work reported in this paper.

Acknowledgements

Research was supported by the National Natural Science Foundation of China (Grant No. 51906031, 51879022), and Fundamental Research Funds for the Central Universities, China.

Appendix A. Supplementary data

Supplementary data to this article can be found online at https://doi.org/10.1016/j.nanoen.2020.104459.

References

[1] S.-M. Lu, A global review of enhanced geothermal system (EGS), Renew. Sustain. Energy Rev. 81 (2018) 2902.
[2] C. Forman, I.K. Muritala, R. Pardemann, B. Meyer, Estimating the global waster heat potential, Renew. Sustain. Energy Rev. 57 (2016) 1568.
[3] S. Chu, A. Majumdar, Opportunities and challenges for a sustainable energy future, Nature 488 (2012) 294.
[4] Z. Yuan, L. Wei, J.D. Afroze, K. Goh, Y. Chen, Y. Yu, Q. She, Y. Chen, Pressure-retarded membrane disstilation for low-grade heat recovery: the critical roles of pressure-induced membrane deformation, J. Membr. Sci. 579 (2019) 90.
[5] L. Miró, J. Gasia, L.F. Cabeza, Thermal energy storage (TES) for industrial waste heat (IWH) recovery: a review, Appl. Energy 179 (2016) 284.
[6] T.C. Hung, Waste heat recovery of organic Rankine cycle using dry fluids, Energy Convers. Manag. 42 (2001) 539.
[7] B.T. Liu, K.H. Chien, C.C. Wang, Effect of working fluids on organic Rankine cycle for waste heat recovery, Energy 29 (2004) 1207.
[8] T.C. Hung, T.Y. Shai, S.K. Wang, A review of organic rankine cycles (ORCs) for the recovery of low-grade waste heat, Energy 22 (1997) 661.
[9] H. Demir, M. Mobedi, S. Ülkü, A review on adsorption heat pump: problems and solutions, Renew. Sustain. Energy Rev. 12 (2008) 2381.
[10] D.M.V.D. Bor, C.A.I. Ferreira, A.A. Kiss, Low grade waste heat recovery using heat pumps and power cycles, Energy 89 (2015) 864.
[11] K.J. Chua, S.K. Chou, W.M. Yang, Advan ces in heat pump systems: a review, Appl. Energy 87 (2010) 3611.
[12] L.E. Bell, Cooling, heating, generating power, and recovering waste heat with thermoelectric systems, Science 321 (2008) 1457.
[13] B. Zhao, P. Santhanam, K. Chen, S. Buddhiraju, S. Fan, Near-field thermophotonic systems for low-grade waste-heat recovery, Nano Lett. 18 (2018) 5224.
[14] X. Gou, H. Xiao, S. Yang, Modeling, experimental study and optimization on low-temperature waste heat thermoelectric generator system, Appl. Energy 87 (2010) 3131.
[15] Q. Leng, L. Chen, H. Guo, J. Liu, G. Liu, C. Hu, Y. Xi, Harvesting heat energy from hot/cold water with a pyroelectric generator, J. Mater. Chem. A 2 (2014) 11940.
[16] M. Rahimi, A.P. Straub, F. Zhang, X. Zhu, M. Elimelech, C.A. Gorski, B.E. Logan, Emerging electrochemical and membrane-based systems to convert low-grade heat to electricity, Energy Environ. Sci. 11 (2018) 276.
[17] S.W. Lee, Y. Yang, H.W. Lee, H. Ghasemi, D. Kraemer, G. Chen, Y. Cui, An electrochemical system for efficiently harvesting low-grade heat energy, Nat. Commun. 5 (2014) 3942.
[18] Y. Yang, J. Loomis, H. Ghasemi, S.W. Lee, Y.J. Wang, Y. Cui, G. Chen, Membrane-free battery for harvesting low-grade thermal energy, Nano Lett. 14 (2014) 6578.
[19] M.J. Moran, H.N. Shapiro, D.D. Boettner, M.B. Bailey, Fundamentals of Engineering Thermodynamics, John Wiley & Sons, 2010.
[20] B.F. Tchanche, G. Papadakis, G. Lambrinos, A. Frangoudakis, Fluid selection for a low-temperature solar organic Rankine cycle, Appl. Therm. Eng. 29 (2009) 2468.
[21] A. Hromádka, Z. Martínek, Overview of the organic Rankine cycles and their current utilization: verification of several current ORCs utilization by the software Dymola, in: International Scientific Conference on Electric Power Engineering, 2017.
[22] I. Sarbu, A review on substitution strategy of non-ecological refrigerants from vapour compression-based refrigeration, air-conditioning and heat pump systems, Int. J. Refrig. 46 (2014) 123.
[23] H. Im, T. Kim, H. Song, J. Choi, J.S. Park, R. Ovalle-Robles, H.D. Yang, K.D. Kihm, R.H. Baughman, H.H. Lee, T.J. Kang, Y.H. Kim, High-efficiency electrochemical thermal energy harvester using carbon nanotube aerogel sheet electrodes, Nat. Commun. 7 (2016) 10600.
[24] A. Gunawan, C.-H. Lin, D.A. Buttry, V. Mujica, R.A. Taylor, R.S. Prasher, P. E. Phelan, Liquid thermoelectrics: review of recent and limited new data of thermogalvanic cell experiments, Nanoscale Microscale Thermophys. Eng. 17 (2013) 304.
[25] C.R. Bowen, J. Taylor, E. LeBoulbar, D. Zabek, A. Chauhan, R. Vaish, Pyroelectric materials and devices for energy harvesting applications, Energy Environ. Sci. 7 (2014) 3836.
[26] Q. Zhang, A. Agbossou, Z. Feng, M. Cosnier, Solar micro-energy harvesting with pyroelectric effect and wind flow, Sens. Actuators, A 168 (2011) 335.
[27] M.-K. Kim, M.-S. Kim, S. Lee, C. Kim, Y.-J. Kim, Wearable thermoelectric generator for harvesting human body heat energy, Smart Mater. Struct. 23 (2014) 105002.
[28] F.Y. Lee, A. Navid, L. Pilon, Pyroelectric waste heat energy harvesting using heat conduction, Appl. Therm. Eng. 37 (2012) 30.
[29] F.-R. Fan, L. Lin, G. Zhu, W. Wu, R. Zhang, Z.L. Wang, Transparent triboelectric nanogenerators and self-powered pressure sensors based on micropatterned plastic films, Nano Lett. 12 (2012) 3109.
[30] Z.L. Wang, J. Chen, L. Lin, Progress in triboelectric nanogenerators as a new energy technology and self-powered sensors, Energy Environ. Sci. 8 (2015) 2250.

[31] Z.L. Wang, Triboelectric nanogenerators as new energy technology and self-powered sensors–Principles, problems and perspectives, Faraday Discuss 176 (2015) 447.
[32] Y. Yang, H. Zhang, G. Zhu, S. Lee, Z.-H. Lin, Z.L. Wang, Flexible hybrid energy cell for simultaneously harvesting thermal, mechanical, and solar energies, ACS Nano 7 (2012) 785.
[33] S. Niu, Z.L. Wang, Theoretical systems of triboelectric nanogenerators, Nano Energy 14 (2015) 161.
[34] X. Cao, Y. Jie, N. Wang, Z.L. Wang, Triboelectric nanogenerators driven self-powered electrochemical processes for energy and environmental science, Adv. Energy Mater. 6 (2016) 1600665.
[35] Y. Jie, Q. Jiang, Y. Zhang, N. Wang, X. Cao, A structural bionic design: from electric organs to systematic triboelectric generators, Nano Energy 27 (2016) 554.
[36] J. Chen, Z.L. Wang, Reviving vibration energy harvesting and self-powered sensing by a triboelectric nanogenerator, Joule 1 (2017) 480, 2017.
[37] G. Zhu, J. Chen, T. Zhang, Q. Jing, Z.L. Wang, Radial-arrayed rotary electrification for high performance triboelectric generator, Nat. Commun. 5 (2014) 3426.
[38] J. Chen, Y. Huang, N. Zhang, H. Zou, R. Liu, C. Tao, X. Fan, Z.L. Wang, Micro-cable structured textile for simultaneously harvesting solar and mechanical energy, Nat. Energy 1 (2016) 16138.
[39] C. Yan, Y. Gao, S. Zhao, S. Zhang, Y. Zhou, W. Deng, Z. Li, G. Jiang, L. Jin, G. Tian, T. Yang, X. Chu, D. Xiong, Z. Wang, Y. Li, W. Yang, J. Chen, A linear-to-rotary hybrid nanogenerator for high-performance wearable biomechanical energy harvesting, Nano Energy 67 (2020) 104235.
[40] Y. Jie, J. Ma, Y. Chen, X. Cao, N. Wang, Z.L. Wang, Efficient delivery of power generated by a rotating triboelectric nanogenerator by conjunction of wired and wireless transmissions using Maxwell's displacement currents, Adv. Energy Mater. 8 (2018) 1802084.
[41] G. Chen, X. Liu, S. Li, M. Dong, D. Jiang, A droplet energy harvesting and actuation system for self-powered digital microfluidics, Lab Chip 18 (2018) 1026.
[42] Z.H. Lin, G. Cheng, S. Lee, K.C. Pradel, Z.L. Wang, Harvesting water drop energy by a sequential contact-electrification and electrostatic-induction process, Adv. Mater. 26 (2014) 4690.
[43] Y. Su, X. Wen, G. Zhu, J. Yang, J. Chen, P. Bai, Z. Wu, Y. Jiang, Z.L. Wang, Hybrid triboelectric nanogenerator for harvesting water wave energy and as a self-powered distress signal emitter, Nano Energy 9 (2014) 186.
[44] M. Xu, S. Wang, S.L. Zhang, W. Ding, P.T. Kien, C. Wang, Z. Li, X. Pan, Z.L. Wang, A highly-sensitive wave sensor based on liquid-solid interfacing triboelectric nanogenerator for smart marine equipment, Nano Energy 57 (2019) 574.
[45] Z.H. Lin, G. Cheng, L. Lin, S. Lee, Z.L. Wang, Water–solid surface contact electrification and its use for harvesting liquid-wave energy, Angew. Chem. Int. Ed. 52 (2013) 12545.
[46] D. Jiang, M. Xu, M. Dong, F. Guo, X. Liu, G. Chen, Z.L. Wang, Water-solid triboelectric nanogenerators: an alternative means for harvesting hydropower, Renew. Sustain. Energy Rev. 115 (2019) 109366.
[47] B.D. Chen, W. Tang, C. He, C.R. Deng, L.J. Yang, L.P. Zhu, J. Chen, J.J. Shao, L. Liu, Z.L. Wang, Water wave energy harvesting and self-powered liquid-surface fluctuation sensing based on bionic-jellyfish triboelectric nanogenerator, Mater. Today 21 (2018) 88.
[48] W. Tang, B.D. Chen, Z.L. Wang, Recent progress in power generation from water/liquid droplet interaction with solid surfaces, Adv. Funct. Mater. (2019) 1901069.
[49] J. Nie, Z. Ren, J. Shao, C. Deng, L. Xu, X. Chen, M. Li, Z.L. Wang, Self-powered microfluidic transport system based on triboelectric nanogenerator and electrowetting technique, ACS Nano 12 (2018) 1491.
[50] J. Nie, X. Chen, Z.L. Wang, Electrically responsive materials and devices directly driven by the high voltage of triboelectric nanogenerators, Adv. Funct. Mater. 29 (2018) 1806351.
[51] J. Nie, Z. Wang, Z. Ren, S. Li, X. Chen, Z.L. Wang, Power generation from the interaction of a liquid droplet and a liquid membrane, Nat. Commun. 10 (2019) 2264.
[52] Y. Zi, L. Lin, J. Wang, S. Wang, J. Chen, X. Fan, P.-K. Yang, F. Yi, Z.L. Wang, Triboelectric–pyroelectric–piezoelectric hybrid cell for high-efficiency energy-harvesting and self-powered sensing, Adv. Mater. 27 (2015) 2340.
[53] S. Wang, Z.L. Wang, Y. Yang, A one-structure-based hybridized nanogenerator for scavenging mechanical and thermal energies by triboelectric–piezoelectric–pyroelectric effects, Adv. Mater. 28 (2016) 2881.
[54] Y. Zi, J. Wang, S. Wang, S. Li, Z. Wen, H. Guo, Z.L. Wang, Effective energy storage from a triboelectric nanogenerator, Nat. Commun. 7 (2016) 10987.
[55] Y. Yang, W. Guo, K.C. Pradel, G. Zhu, Y. Zhou, Y. Zhang, Y. Hu, L. Lin, Z.L. Wang, Pyroelectric nanogenerators for harvesting thermoelectric energy, Nano Lett. 12 (2012) 2833.
[56] N. Ma, Y. Yang, Enhanced self-powered UV photoresponse of ferroelectric BaTiO3 materials by pyroelectric effect, Nano Energy 40 (2017) 352.
[57] Y. Yang, J.H. Jung, B.K. Yun, F. Zhang, K.C. Pradel, W. Guo, Z.L. Wang, Flexible pyroelectric nanogenerators using a composite structure of lead-free KNbO3 nanowires, Adv. Mater. 24 (2012) 5357.
[58] Y. Yang, S. Wang, Y. Zhang, Z.L. Wang, Pyroelectric nanogenerators for driving wireless sensors, Nano Lett. 12 (2012) 6408.
[59] Y. Wu, X. Wang, Y. Yang, Z.L. Wang, Hybrid energy cell for harvesting mechanical energy from one motion using two approaches, Nano Energy 11 (2015) 162.
[60] X. Wen, Y. Su, Y. Yang, H. Zhang, Z.L. Wang, Applicability of triboelectric generator over a wide range of temperature, Nano Energy 4 (2014) 150.
[61] K. Zhang, S. Wang, Y. Yang, A one-structure-based piezo-tribo-pyro-photoelectric effects coupled nanogenerator for simultaneously scavenging mechanical, thermal, and solar energies, Adv. Energy Mater. 7 (2017) 1601852.
[62] Y. Ji, K. Zhang, Y. Yang, A one-structure-based multieffects coupled nanogenerator for simultaneously scavenging thermal, solar, and mechanical energies, Adv. Sci. 5 (2018) 1700622.
[63] Y. Yang, Z.-H. Lin, T. Hou, F. Zhang, Z.L. Wang, Nanowire-composite based flexible thermoelectric nanogenerators and self-powered temperature sensors, Nano Res 5 (2012) 888.
[64] Y. Yang, H. Zhang, X. Zhong, F. Yi, R. Yu, Y. Zhang, Z.L. Wang, Electret film-enhanced triboelectric nanogenerator matrix for self-powered instantaneous tactile imaging, ACS Appl. Mater. Interfaces 6 (2014) 3680.
[65] S.-H. Kwon, J. Park, W.K. Kim, Y. Yang, E. Lee, C.J. Han, S.Y. Park, J. Lee, Y.S. Kim, An effective energy harvesting method from a natural water motion active transducer, Energy Environ. Sci. 7 (2014) 3279.
[66] J.K. Moon, J. Jeong, D. Lee, H.K. Pak, Electrical power generation by mechanically modulating electrical double layers, Nat. Commun. 4 (2013) 1487.
[67] S.-B. Jeon, D. Kim, G.-W. Yoon, J.-B. Yoon, Y.-K. Choi, Self-cleaning hybrid energy harvester to generate power from raindrop and sunlight, Nano Energy 12 (2015) 636.
[68] S.-H. Kwon, W.K. Kim, J. Park, Y. Yang, B. Yoo, C.J. Han, Y.S. Kim, Fabric active transducer stimulated by water motion for self-powered wearable device, ACS Appl. Mater. Interfaces 8 (2016) 24579.
[69] F. Gao, W. Li, X. Wang, X. Fang, M. Ma, A self-sustaining pyroelectric nanogenerator driven by water vapor, Nano Energy 22 (2016) 19.
[70] G. Cha, Y.S. Ju, Pyroelectric energy harvesting using liquid-based switchable thermal interfaces, Sens. Actuators, A 189 (2013) 100.
[71] R. Hasegawa, Y. Takahashi, Y. Chatani, H. Tadokoro, Crystal structures of three crystalline forms of poly(vinylidene fluoride), Polym. J. 3 (1971) 600.
[72] B.B. Owen, R.C. Miller, C.E. Milner, H.L. Cogan, The Dielectric constant of water as a function of temperature and pressure, J. Phys. Chem. 65 (1961) 2065.
[73] L.E. Helseth, X.D. Guo, Hydrophobic polymer covered by a grating electrode for converting the mechanical energy of water droplets into electrical energy, Smart Mater. Struct. 25 (2016), 045007.
[74] J. Cui, X. Chen, F. Wang, X. Gong, Z. Yu, Study of liquid droplets impact on dry inclined surface, Asia-Pacific, J. Chem. Eng. 4 (2009) 643.
[75] J.K. Beattie, A.M. Djerdjev, A. Gray-Weale, N. Kallay, J. Lützenkirchen, T. Preočanin, A. Selmani, pH and the surface tension of water, J. Colloid Interface Sci. 422 (2014) 54.
[76] R. Tuckermann, Surface tension of aqueous solutions of water-soluble organic and inorganic compounds, Atmos. Environ. 41 (2007) 6265.
[77] G. Jones, S.K. Talley, The viscosity of aqueous solutions as a function of the concentration, J. Am. Chem. Soc. 55 (1933) 624.
[78] B.D. Chen, W. Tang, C. He, T. Jiang, L. Xu, L.P. Zhu, G.Q. Gu, J. Chen, J.J. Shao, J. J. Luo, Z.L. Wang, Ultrafine capillary-tube triboelectric nanogenerator as active sensor for microliquid biological and chemical sensing, Adv. Mater. Technol. 3 (2018) 1700229.
[79] L. Pan, J. Wang, P. Wang, R. Gao, Y.-C. Wang, X. Zhang, J.-J. Zou, Z.L. Wang, Liquid-FEP-based U-tube triboelectric nanogenerator for harvesting water-wave energy, Nano Res 11 (2018) 4062.
[80] D. Jiang, F. Guo, M. Xu, J. Cai, S. Cong, M. Jia, G. Chen, Y. Song, Conformal fluorine coated carbon paper for an energy harvesting water wheel, Nano Energy 58 (2019) 842.
[81] Y. Wu, Y. Su, J. Bai, G. Zhu, X. Zhang, Z. Li, Y. Xiang, J. Shi, A self-powered triboelectric nanosensor for PH detection, J. Nanomater. 2016 (2016) 1.

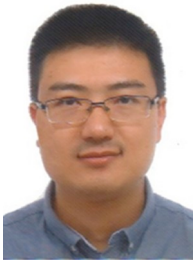

Dongyue Jiang received his Ph.D degree in National University of Singapore. Now he is an Associate Professor in School of Energy and Power, Dalian University and Technology. His research interests include: Water-solid triboelectric nanogenerators, TENG based actuators, electrowetting *etc*.

Yunpeng Su received his Bachelor's degree from Lanzhou Jiaotong University. Now he is a Master candidate in Prof. Dongyue Jiang and Prof. Guijun Chen's group in Dalian University of Technology. His research focus on triboelectric nanogenerators, solar energy storage and heat utilization.

Kun Wang received his Bachelor's degree from Shandong University of Technology. Now he is a Master candidate in Prof. Dongyue Jiang and Prof. Guijun Chen's group in Dalian University of Technology. His research direction is water-solid triboelectric nanogenerators, energy harvesting and conversion.

Yutao Wang received his Bachelor's degree in North China Electric Power University. Now he is a Master candidate in Prof. Dongyue Jiang and Guijun Chen's group in Dalian University of Technology. His research interests includes triboelectric nanogenerators and self-powered liquid actuators.

Minyi Xu received his Ph.D degree from Peking University. Now he is a Full Professor in Dalian Maritime University. His research interests include water wave related TENG devices in applications such as intelligent shipping and so on.

Ming Dong received his Ph.D degree in Dalian University of Technology. Now he is a Full Professor in Dalian University of Technology. His research interests includes solid-gas two phase flow and dust elimination *etc*.

Guijun Chen is an Associate Professor in Dalian University of Technology. His research interests include modelling and analysis of thermal energy systems including boilers, heat exchangers, recycling of condensate water and so on.